We appreciate the reviewer for the useful comments. In the following, original reviewer comments are shown in black, our point-by-point responses are shown in blue, and updates on the manuscript are highlighted in yellow.

**Reviewer: 1**

**General comments:**

The authors investigate the transport and transformation of atmospheric reactive nitrogen (Nr), specifically particulate ammonium ($pNH_4^+$) and nitrate ($pNO_3^-$), in a mountain forest environment at Xitou, Taiwan, using size-resolved isotope measurements combined with Bayesian modeling. Samples were collected over a one-week period from April 7 to April 14, 2021, with daytime (09:00–17:00 LT) and nighttime (18:00–06:00 LT) samples analyzed separately. During this period, approximately 26 hours of fog occurred under stagnant atmospheric conditions.

Size-segregated isotope analyses were conducted on these diurnally collected filter samples, although such measurements are technically challenging because of low particle concentrations. The $\delta^{15}N$ and $\delta^{18}O$ isotope measurements were performed using gas chromatography–isotope ratio mass spectrometry (GC-IRMS), and the resulting isotope data were used to infer source contributions and nitrate formation pathways through Bayesian analysis.

Based on the observation that both $\delta^{15}N$–$NH_4^+$ and $\delta^{15}N$–$NO_3^-$ decreased during the extended fog event, the authors suggest that the decreasing was associated with fog processes. They further suggest that urban plumes retain $O_3$-driven oxidation signatures, whereas nitrate formed locally in the mountain environment shows greater influence from $RO_2$-involved chemistry and biogenic contributions. Bayesian modeling further indicates that 50–83% of $NH_3$ emissions are combustion-related, while 42–95% of $pNO_3^-$ is attributed to $RO_2$-initiated oxidation during daytime and 6–84% to heterogeneous reactions at night.

**R1C1:**

However, in comparison with previous studies conducted at the same site and in the same region and other locations worldwide (Fig S9, S10), Lee et al. (2025) largely corroborates earlier conclusions regarding urban influence, fog/cloud processing, and secondary oxidation involving $RO_2/O_3$ and isotopic dilution during transport but provides limited additional mechanistic insight.

Response:

We agree with the reviewer that additional mechanistic insight would be needed when comparing with earlier datasets. This part was updated in section 3.3.1 (Lines 241−248) and 3.4.2 (Lines 363−373) of the revised manuscript as follows:

> (Lines 241−248) "The daily concentration-weighted $\delta^{15}N$-$NH_4^+$ values at the Xitou site ranged from 6.31‰ to 14.69‰, with an average of 10.95 ± 2.76‰ (Fig. 2f, calculation details in Supplementary Description S5). These results are consistent with previous winter observations at this site (−3.7‰ to 21.39‰, with an average of 11.95 ± 2.65‰) (Chen et al., 2022). As shown in Fig. S5, these values fall between those typical of urban-influenced environments (19.6‰) and remote/forest sites (~5.6‰), reflecting the mixed-source characteristics of Xitou (Chen et al., 2022; Kawashima et al., 2023; Hall et al.,

2016; Kundu et al., 2010; Moore, 1977; Proemse et al., 2012; Savard et al., 2017; Ti et al., 2018; Walters et al., 2022). The isotopic signature is particularly comparable to other semi-rural receptor sites in East Asia that receive diluted urban plumes mixed with regional agricultural background."

(Lines 363−373) "The daily concentration-weighted $\delta^{18}O\text{-}NO_3^-$ ranged from 30.98 to 73.27‰, with an average value of 51.82±16.47‰ (Fig. 2h). Similar to $\delta^{15}N\text{-}NO_3^-$, these values align with measurements from other mountain regions such as 10.8−92.4‰ at Mt. Lulin (Guha et al., 2017) and 64.71±11.52‰ at the Himalayan-Tibetan Plateau (Lin et al., 2021), but are lower than previous winter observations (72.66±3.42‰) (Chen et al., 2022), as illustrated in Fig. S11. In contrast, $\delta^{18}O\text{-}NO_3^-$ at urban sites such as Changchun (68.16±9.52‰) and Beijing (83.8±13.4‰) are substantially higher, consistent with $O_3$-dominated oxidation under polluted conditions. The relatively lower $\delta^{18}O\text{-}NO_3^-$ values at Xitou and other mountain sites suggest that $RO_2$-initiated pathways contribute more substantially to nitrate formation under less-polluted conditions. A sharp decrease in $\delta^{18}O\text{-}NO_3^-$ from 70.44‰ (18D) to 33.81‰ (18N and 19D) occurred during the fog, coinciding with $\delta^{15}N\text{-}NO_3^-$ depletion. This shift from $O_3$- to $RO_2$-dominated oxidation, is likely driven by stagnant winds, suppressed urban input, and enhanced local aqueous-phase chemistry under high RH."

**R1C2:** The isotopic effects induced by fog/cloud aqueous-phase processing and those associated with long-range transport act in the same direction, making it difficult to disentangle their respective contributions based on the presented data.

Response: We appreciate the reviewer's point regarding the potential overlap between transport-related isotopic shifts and those induced by fog processing. We have revised the manuscript to clarify these mechanisms and address the terminology used.

For the terminology, we would like to clarify that the term "long-range transport" was used imprecisely in the original manuscript to describe the movement of air plumes from urban areas to our sampling site via upslope valley winds and sea breezes. We acknowledge that this does not align with the standard atmospheric definition of long-range transport, which typically implies distances of hundreds to thousands of kilometers. We have corrected this terminology throughout the revised manuscript.

During transport of urban air plumes, particles are expected to carry relatively elevated $\delta^{15}N$ signatures, reflecting their combustion-related origin. As the plume travels toward the site, ongoing gas-particle partitioning progressively depletes the heavier isotopes from the gas phase (NOx and $NH_3$), causing the $\delta^{15}N$ of both gas and particle phases to decline over transport distance. During fog events, two concurrent processes likely contribute to lower $\delta^{15}N$ values in $pNH_4^+$ and $pNO_3^-$. First, weak wind conditions suppress the advection of urban-influenced air with higher $\delta^{15}N$, reducing the contribution of combustion-derived nitrogen. Second, hygroscopic growth and wet deposition of existing particles drive the uptake of ambient NOx and $NH_3$ into the particle phase to maintain ionic charge balance. These gases carry relatively low $\delta^{15}N$ values, reflecting (1) their partly agricultural origin, or (2) the isotopic fractionation they have already undergone during transport. Their incorporation into the particle phase, therefore, further lowers the bulk $\delta^{15}N$ of $pNH_4^+$ and $pNO_3^-$. We acknowledge that, given the current dataset, the relative contributions of these two processes cannot be quantitatively

separated. Targeted laboratory studies on the isotopic effects of aqueous-phase reactions involving $pNH_4^+$ and $pNO_3^-$ will be necessary to disentangle these mechanisms in future work. This part was updated in section 3.3.1 in the revised manuscript (Lines 251−256) as follows:

> (Lines 251−256) "[…] This decline of $\delta^{15}N$ during the fog likely results from three concurrent processes under stagnant conditions. First, stagnant conditions suppressed the transport of $\delta^{15}N$-enriched urban plumes from nearby source regions. Second, continuous exchange between gas-phase $NH_3$ and $pNH_4^+$ shifts the particle phase toward the signature of the local $NH_3$ pool, which is depleted in $\delta^{15}N$ due to agricultural volatilization. Furthermore, wet deposition during fog may remove $^{15}N$-enriched particles, forcing the remaining $pNH_4^+$ to re-equilibrate with an increasingly $\delta^{15}N$-depleted gas phase. […]"

**R1C3:** Furthermore, the Bayesian source apportionment using MixSIAR relies on multiple layers of assumptions, including (1) the recalculation of $\delta^{15}N$–$NH_3$ from particulate $NH_4^+$ based on assumed fractionation factors ($\varepsilon(NH_3–NH_4^+)$), temperature dependence, gas–particle equilibrium, and the approximation of an open systems equilibrium, and (2) the selection of source endmember isotope signatures. Consequently, the posterior distributions are broad and show substantial overlap, between clear & foggy conditions, during both daytime & nighttime (Fig. 5 (b)). Although the modeling framework is internally consistent, it does not yield unique or well-constrained source attribution or oxidation pathway estimates.

Response: We thank the reviewer for this critical point. The influences of (1) temperature, (2) gas-particle equilibrium, and (3) the assumption of equilibrium in open systems on $\varepsilon(NH_3–NH_4^+)$ were discussed step by step as follows:

First, the influence of temperature on $\varepsilon(NH_3–NH_4^+)$ was estimated using an empirical relationship as follows (Kawashima et al., 2023):

$$\varepsilon_{\left(NH_4^+-NH_3\right)} = \frac{12.4678\times 1000}{\left(T+273.15\right)} - 7.6694,$$

where $T$ represents temperature in °C. Since the temperature measured in Xitou ranged from 10−30°C, the resulting differences in $\varepsilon(NH_3–NH_4^+)$ ranged from 36.36 (at 10°C) to 33.46 (at 30°C), and the contribution of each emission source estimated by MixSIAR is shown as follows:

| Contribution (%) | Fertilizer | Fossil Fuel | $NH_3$ slip | waste |
|---|---|---|---|---|
| $\varepsilon$ ($NH_3–NH_4^+$) = 33 ‰ | 4.2 ± 3.2 | 66.4 ± 15.1 | 23.2 ± 18.3 | 5.2 ± 5 |
| $\varepsilon$ ($NH_3–NH_4^+$) = 37 ‰ | 4.6 ± 3.8 | 42.3 ± 18.7 | 46 ± 23 | 7.1 ± 6.1 |

The estimated contributions for fertilizer and waste at 10 and 30°C are similar. The most different part is the contribution from fossil fuel, which was estimated to decrease by ~ 20% at higher temperatures. In contrast, the contribution for $NH_3$ slip was estimated to increase by ~ 20% at higher temperatures.

Second, sensitivity tests on (1) nucleation with a kinetic isotope effect (KIE) of −28‰, (2) $NH_{3(aq)}/NH_{3(g)}$ chemical equilibrium during condensation (equilibrium isotope effect (EIE) of 4 ± 3‰), and (3) $NH_4^+{}_{(aq)}/NH_{3(aq)}$ chemical equilibrium during condensation (EIE of 37 ± 4‰), were

added to address the influence of gas-particle equilibrium, in additional to the original single isotope fractionation reaction ($NH_4^+{}_{(aq/s)}/NH_{3(g)}$ chemical equilibrium during condensation (EIE of 33‰)) (Chang et al., 2025). It is possible to estimate the contribution of each reaction if we know the $\delta^{15}N$ of $NH_3$. Unfortunately, since the values of $\delta^{15}N$-$NH_3$ were not measured in this study, we relied on the estimation of fractionation factors to estimate $\delta^{15}N$-$NH_3$. Here, we assume each reaction contributed 100% and performed several sensitivity tests. The results are organized as follows:

| Contribution (%) | Fertilizer | Fossil Fuel | $NH_3$ slip | waste |
|---|---|---|---|---|
| KIE (−28 ‰) | 26.6 ± 34 | 12.6 ± 10.4 | 56.3 ± 35.4 | 4.6 ± 4.4 |
| EIE (4 ‰) | 1.8 ± 1.9 | 21.1 ± 15.3 | 74.3 ± 15.4 | 2.8 ± 2.9 |
| EIE (33 ‰) | 4.2 ± 3.2 | 66.4 ± 15.1 | 23.2 ± 18.3 | 5.2 ± 5 |
| EIE (37 ‰) | 4.6 ± 3.8 | 42.3 ± 18.7 | 46 ± 23 | 7.1 ± 6.1 |

When assuming equilibrium, contributions of fertilizer and waste range from 1.8 to 4.6%, and 2.8 to 7.1%, respectively. For fossil fuel and $NH_3$ slip, the contributions range from 21.1 to 66.4%, and 23.2 to 74.3%, respectively. However, when only considering KIE, the contribution of fertilizer increased to 26.6%, fossil fuel decreased to 12.6%, while the contribution of $NH_3$ slip and waste is still within the range of EIE effects. Despite this sensitivity, the combined contribution of fossil fuel and $NH_3$ slip remains dominant (88–95%) across all equilibrium scenarios (EIE = 4, 33, 37‰), suggesting that the qualitative conclusion that anthropogenic $NH_3$ sources dominate particulate ammonium at Xitou is robust to the choice of fractionation factor.

The KIE scenario (nucleation-dominated) represents a physically extreme end-member. At Xitou, $NH_4^+$ formation is dominated by condensation under open-system conditions, where $NH_{3(g)}$ is in continuous exchange with the gas phase rather than being irreversibly incorporated. Under such conditions, isotope fractionation approaches thermodynamic equilibrium (EIE) rather than kinetic control (KIE). The KIE result is therefore interpreted as an upper bound on uncertainty rather than a likely atmospheric condition. We acknowledge that the absolute partitioning between fossil fuel combustion and $NH_3$ slip remains uncertain under the current framework, and this limitation has been explicitly stated in section 3.3.2 of the revised manuscript (Lines 307−310).

(Lines 307−310) "[…] Despite the sensitivity of $\varepsilon_{NH_4^+-NH_3}$ to temperature (Kawashima et al., 2023) and gas−particle equilibrium (Chang et al., 2025), the estimated $\delta^{15}N$-$NH_3{}^0$ consistently yielded MixSIAR results in which combustion-related sources accounted for 88–95% of total $NH_3$ emission (see Supplementary Description S3 and Table S1). […]"

"**Description S3 Sensitivity analyses on $\varepsilon_{NH_4^+-NH_3}$**

The influence of (1) temperature, (2) gas−particle equilibrium, and (3) open-system equilibrium assumptions on $\varepsilon_{NH_4^+-NH_3}$ is discussed below.

**Temperature dependence.** The temperature sensitivity of $\varepsilon_{NH_4^+-NH_3}$ was estimated using the empirical relationship of Kawashima et al. (2023):

$$\varepsilon_{NH_4^+-NH_3} = \frac{12.4678\times 1000}{(T+273.15)} - 7.6694, \quad \text{(S1)}$$

where $T$ represents temperature in °C. Over the observed temperature range at Xitou (10−30°C), $\varepsilon_{NH_4^+-NH_3}$ varied from 36.36‰ (at 10°C) to 33.46‰ (at 30°C). MixSIAR source contributions estimated at these two temperature extremes are summarized in Table S1 ($\varepsilon_{NH_4^+-NH_3}$ of 33‰ and 37‰). Contributions from fertilizer and waste were insensitive to temperature. The most notable temperature effect was on fossil fuel and $NH_3$ slip: the fossil fuel contribution decreased by ~ 20% at higher temperature, while $NH_3$ slip increased correspondingly by ~ 20%.

**Gas−particle equilibrium fractionation pathways.** In addition to the baseline fractionation reaction ($NH_4^+{}_{(aq/s)}/NH_{3(g)}$ equilibrium during condensation (equilibrium isotope effect (EIE) of 33‰), three alternative fractionation scenarios were tested: (1) nucleation with a kinetic isotope effect (KIE) of −28‰, (2) $NH_{3(aq)}/NH_{3(g)}$ equilibrium during condensation (EIE of 4 ± 3‰), and (3) $NH_4^+{}_{(aq)}/NH_{3(aq)}$ equilibrium during condensation (EIE = 37 ± 4‰) (Chang et al., 2025). Because $\delta^{15}N\text{-}NH_3$ was not directly measured in this study, $\delta^{15}N\text{-}NH_3$ was inferred from fractionation factors rather than observation. Each scenario was therefore evaluated independently under the assumption that it contributed 100% to $NH_3$ formation, and the resulting MixSIAR source contributions are reported in Table S1.

Under equilibrium fractionation scenarios (EIE = 4, 33, 37‰), contributions from fertilizer and waste ranged from 1.8–4.6% and 2.8–7.1%, respectively, while fossil fuel and $NH_3$ slip ranged from 21.1–66.4% and 23.2–74.3%, respectively. The combined contribution of fossil fuel and $NH_3$ slip remained dominant across all EIE scenarios (88–95%), indicating that the qualitative conclusion that "anthropogenic $NH_3$ sources dominate particulate ammonium at Xitou" is robust to the choice of equilibrium fractionation factor.

**Open-system equilibrium assumptions.** Under the KIE scenario, the estimated fertilizer contribution increased to 26.6%, and fossil fuel decreased to 12.6%, while $NH_3$ slip and waste remained within the range spanned by EIE scenarios. However, the KIE scenario represents a physically extreme end-member. At Xitou, $NH_3$ formation is dominated by condensation under open-system conditions, where $NH_{3(g)}$ undergoes continuous exchange with the gas phase rather than irreversible incorporation. Under such conditions, isotope fractionation is expected to approach thermodynamic equilibrium (EIE) rather than kinetic control (KIE). The KIE result is therefore best interpreted as an upper bound on source apportionment uncertainty rather than a physically realistic atmospheric scenario."

**Table S1.** Sensitivity of gas−particle equilibrium in estimating $NH_3$ emission sources.

| $\varepsilon_{NH_4^+-NH_3}$ | Contribution (%) | | | |
|---|---|---|---|---|
| | Fertilizer | Fossil Fuel | $NH_3$ slip | waste |
| −28 ‰ | 26.6 ± 34 | 12.6 ± 10.4 | 56.3 ± 35.4 | 4.6 ± 4.4 |
| 4 ‰ | 1.8 ± 1.9 | 21.1 ± 15.3 | 74.3 ± 15.4 | 2.8 ± 2.9 |
| 33 ‰ | 4.2 ± 3.2 | 66.4 ± 15.1 | 23.2 ± 18.3 | 5.2 ± 5 |
| 37 ‰ | 4.6 ± 3.8 | 42.3 ± 18.7 | 46 ± 23 | 7.1 ± 6.1 |

Regarding the source endmember isotope signatures, we followed the selection of Kawashima et al. (2023), which compiled $\delta^{15}N\text{-}NH_3$ source data from 15 references with passive sampler

corrections applied. The four source categories and their $\delta^{15}N$-$NH_3$ values are: fertilizer (−34.1 to −22.5‰, n = 21), waste (−23.2 to −12‰, n = 51), $NH_3$ slip (−13.7 to −2.7‰, n = 9), and fossil fuel combustion (−1.4 to 5‰, n = 38). These four categories span a range of ~30‰ with inter-category separation consistently exceeding the within-category standard deviation, providing sufficient isotopic contrast for MixSIAR to distinguish source contributions. We acknowledge that the differences between clear & foggy conditions, during both daytime & nighttime, can be similar. We removed that original statement that "Source dynamics varied significantly with isotopic shifts", and updated it in section 3.3.2 (Lines 314−319) of the revised manuscript:

> (Lines 314−319) "[…] It should be noted, however, that the differences in source contributions between daytime and nighttime periods, or between fog and clear conditions, remain within the overlapping ranges of the posterior distributions; consequently, the current sample number precludes statistically robust discrimination between these conditions. Expanded measurements encompassing multiple seasons and contrasting meteorological regimes would be necessary to establish whether systematic diurnal or fog-driven shifts in $NH_3$ source apportionment exist at this site."

**R1C4:** In addition, the linkage between fog events and isotopic variations appears weak, based on Fig. 2. Although uncertainties are not explicitly provided, low values of $\delta^{15}N$–$NH_4^+$, $\delta^{15}N$–$NO_3^-$, and $\delta^{18}O$–$NO_3^-$ also occur outside foggy periods. Therefore, the observed decreases in isotopic values are not unique to fog events, contrary to the authors' interpretation.

Response: We thank the reviewer for this point. We agree that low isotopic values are not exclusively restricted to foggy periods. However, while these signatures are not unique to fog, the fog period represents a period where multiple isotope-depleting mechanisms occur simultaneously. Specifically, during fog events: (1) wet scavenging preferentially removes aerosol particles that have accumulated $^{15}N$-enriched nitrogen from urban areas, reducing the $^{15}N$ source signal in the residual particle phase; (2) the scavenged aerosol undergoes re-equilibration with gas-phase $NH_3$, which is depleted in $^{15}N$ relative to particulate $NH_4^+$, driving $\delta^{15}N$-$NH_4^+$ toward lower values; and (3) nitrate formation pathway shifted toward $RO_2$-initiated pathways that produce nitrate with lower $\delta^{18}O$.

In contrast, the low isotopic values observed outside fog periods likely reflect individual, single-mechanism perturbations. For instance, low $\delta_{15}N$-$NH_4^+$ during clear periods may occur when the source contribution shifts toward agricultural $NH_3$ emissions (e.g., 21D), which carry inherently lower $\delta^{15}N$ signatures. Similarly, decreases in $\delta^{15}N$-$NO_3^-$ and $\delta^{18}O$-$NO_3^-$ during non-fog periods are consistent with transient shifts in nitrate formation pathways or local isotope fractionation, but these may not be reinforced by the concurrent scavenging and re-equilibration dynamics that characterize fog events.

We have revised the relevant text in Section 3.3.1 (Lines 278−281) and 3.4.1 (Lines 337−342) to clarify that fog events are associated with the convergence of these mechanisms rather than being the sole condition under which low isotopic values occur.

> (Lines 278−281) "During fog, the bell-shaped distribution flattened significantly. Weakened wind suppressed the upslope transport of enriched anthropogenic pollutants, while enhanced aqueous-phase interaction promoted uniform isotopic re-equilibrium across all sizes. The high $NO_3^-$ concentration from aqueous chemistry can also promote

the local isotopically depleted $NH_3$ partitioning into the particle phase, dampening the size-dependent isotopic gradient."

(Lines 337−342) "[…] During the fog, $\delta^{15}N\text{-}NO_3^-$ decreased significantly from −2.19‰ (18D) to −4.80‰ (18N), and further to −6.54‰ (19D) (Fig. 2g). This decline, contrasting with previous shorter fog events (Chen et al., 2022), reflects the combined effects of prolonged stagnation and a reduced influx of urban air. These conditions promote enhanced aqueous-phase $pNO_3^-$ formation, predominantly driven by $\delta^{15}N$-depleted $NO_x$ from locally derived biogenic precursors or precursors that have undergone extensive fractionation during transport (Vicars et al., 2013; Gobel et al., 2013)."

We have also added some brief discussions of the non-fog low-value occurrences to provide a more complete mechanistic picture in Section 3.3.1 (Lines 282−289) and Section 3.4.1 (Lines 343−351).

(Lines 282−289) "The flat $\delta^{15}N\text{-}NH_4^+$ size distribution was also observed on 19N and 21D. For 19N, it is likely a legacy effect of the preceding fog period (18D, 18N, and 19D). The $NH_3$ pool remained isotopically depleted from sustained fog-driven scavenging and re-equilibration, and regional transport had not yet replenished the accumulation-mode signal. However, high sub-micrometer $NO_3^-$ concentration (Fig. S4) suggests that fog-like aqueous chemistry persisted, maintaining isotopic signatures similar to 18D. Conversely, the flat distribution on 21D reflects a distinct source influence. HYSPLIT back-trajectories (Fig. S7) indicate that the air parcel traveled through agricultural regions characterized by heavily depleted $NH_3$ (e.g., livestock waste, −28.3‰ to −17.6‰). The partitioning of this isotopically light $NH_3$ during transit effectively erased the characteristic accumulation-mode enrichment."

(Lines 343−351) "Relatively low concentration-weighted $\delta^{15}N\text{-}NO_3^-$ values observed outside the fog periods on 20N and 22N, likely attributable to distinct mechanisms. For 22N, the depletion is linked to enhanced local production, supported by elevated sub-micrometer $NO_3^-$ concentration shown in Fig. S4. For 22N, the low $\delta^{15}N$ coincides with significant deposition loss, as evidenced by low total $NO_3^-$ levels (Fig. S4b). Because $HNO_3$ readily reacts with coarse-mode mineral dust and sea salt, the deposition efficiency during transport is high; this preferential removal of $\delta^{15}N$-enriched species often leaves the residual nitrate pool isotopically lower. Furthermore, the thermodynamic partitioning of $HNO_3$, governed by ambient temperature and particle acidity regulated by sulfate and ammonium, critically influences the observed $\delta^{15}N$. Ultimately, the observed $\delta^{15}N$ at this site serves as an integrated signal of physical and chemical dynamics processes within the air parcel during its transit."

**R1C5:** Finally, there is room to improve the overall organization and logical flow of the manuscript. The presentation is overly dense in places and lacks clear structural connections between sections, which hinders the clarity of the scientific narrative.

Response: We thank the reviewer for this feedback. We have made substantial revisions to the organization and logical flow throughout the manuscript. Specifically, the introduction has been restructured to more clearly establish research gaps and motivate the study objectives; and the discussion has been rewritten to more explicitly connect isotopic observations to process-level

interpretations, with transitional sentences linking each subsection to the overarching scientific narrative. We believe these revisions have improved the readability and coherence of the manuscript as a whole.

**R1C6:** Overall, the study primarily reinforces existing understanding rather than advancing new conceptual or methodological developments in atmospheric nitrogen isotope analysis. Therefore, it may not be well suited for publication in ACP, and submission to a more appropriate journal is recommended.

We thank the reviewer for this feedback. After addressing the reviewer's comments, we believe that this study offers advances across three perspectives:

**Methodological novelty.** This study is among the first to apply size-resolved dual-isotope analysis ($\delta^{15}N$ and $\delta^{18}O$) simultaneously to both $pNH_4^+$ and $pNO_3^-$ in a mountain cloud forest setting, where the majority of isotope-based Nr studies rely on bulk $PM_{2.5}$ or $PM_{10}$ samples due to limited sample mass available at such sites. Size-resolved measurements provide mechanistic information on size-dependent nitrogen transformation that bulk approaches cannot resolve.

**Novel observational findings.** We document two previously unreported behaviors. First, a systematic flattening of the bell-shaped size-resolved $\delta^{15}N$-$NH_4^+$ distribution during the prolonged fog episode, attributed to aqueous-phase gas–particle isotopic re-equilibration and wet scavenging that suppressed the accumulation-mode isotopic enrichment characteristic of clear-period urban plume transport. Second, a $\delta^{15}N$–$\delta^{18}O$ analysis of $pNO_3^-$ identifies at least two co-existing nitrate formation pathways ($O_3$-initiated vs. $RO_2$-initiated) and reveals a systematic shift toward $RO_2$-dominated production during fog. This transition was not previously quantified using isotopic approaches at subtropical mountain sites.

**Site and process novelty.** Xitou represents an under-characterized regime in East Asian Nr research: a subtropical cloud forest situated in a valley that channels urban-to-rural plume transport under persistently high-humidity conditions. By integrating size-resolved isotopes with MixSIAR Bayesian source apportionment, we quantify source contributions (combustion-related $NH_3$: 50–83%) and formation pathway partitioning ($pNO_3^-$ via $RO_2$-initiated oxidation: 42–95% daytime; heterogeneous reactions: 6–84% nighttime) at a site where biogenic and anthropogenic Nr interact in ways not previously characterized. These results carry implications beyond the study site, suggesting that even in remote or rural environments, combustion-related sources can dominate ammonium loading, and that $RO_2$-initiated pathways may be systematically underweighted in current Nr budgets for mountain regions.

We believe these contributions represent new findings rather than confirmations of prior work. They directly address ACP's stated scope for aerosol process studies, specifically aerosol microphysics, chemical composition, and transformation processes. We have strengthened the framing of these contributions in the revised Introduction and Discussion.

**Specific comments**

**R1C7:** L134-L136: Please clarify the primary scale used for $\delta^{15}N$ and $\delta^{18}O$ (e.g., air-$N_2$, VMOW or others). It is recommended to include the weblink for both international isotope reference materials (USGS 34 and IAEA-NO3)

Response: We thank the reviewer for this point. The primary scale used for $\delta^{15}N$ and $\delta^{18}O$, as well as the weblink for the two international isotope references, were added to the introduction section of the revised manuscript (Lines 59−63) as follows:

> (Lines 59−63) "[…] Nitrogen isotope ratios ($\delta^{15}N = [(^{15}R_{sample})/(^{15}R_{air}) - 1] \times 1000‰$, where $^{15}R$ is the ratio of $^{15}N/^{14}N$) are used to distinguish emission sources of $p\mathrm{NH_4^+}$ and transport of $p\mathrm{NO_3^-}$ (Savard et al., 2017; Chang et al., 2018), while oxygen isotope ratios ($\delta^{18}O = [(^{18}R_{sample})/(^{18}R_{VSMOW}) - 1] \times 1000‰$, where $^{18}R$ is the ratio of $^{18}O/^{16}O$) in $p\mathrm{NO_3^-}$ provide insights into specific oxidation pathways, as each oxidant ($O_3$, OH, $RO_2$) imparts a unique isotopic fingerprint (Walters and Michalski, 2016). […]"

**R1C8:** L181-L199: The description in this section is confusing and difficult to follow.

Response: We appreciate the reviewer for pointing out the issue. We agree that the original naming of nitrate formation pathways (P1a, P2a, P3a, P1b, P2b, and P3b) was not easy to follow. We updated the naming in this section and provided explanations for these reactions in the introduction. This point was updated in the introduction (Lines 45−46, 52−54) and method sections (Lines 173−183) of the revised manuscript as follows.

> (Lines 45−46) "[…] In the presence of sunlight, $NO_x$ undergoes rapid oxidation through ozone ($O_3$) or peroxy radical ($RO_2$) pathways (termed $P_{O_3}$ and $P_{RO_2}$, respectively) before converting to nitric acid ($HNO_3$) via the following reactions: […]"
>
> (Lines 52−54) "[…] Under nocturnal or low-light conditions, $NO_x$ accumulates as nitrogen dioxide ($NO_2$) through reaction with $O_3$, which then undergoes heterogeneous reactions (termed as het) to produce $HNO_3$ as follows: […]"
>
> (Lines 173−183) "$\delta^{18}O\text{-}NO_3^-$ is applied to evaluate the relative contributions of various $HNO_3$ formation. Six potential pathways were considered by combining the primary oxidants ($P_{O_3}$ and $P_{RO_2}$) with three terminal mechanisms (OH1, OH2, and heterogeneous processes (het)). These pathways are characterized by their specific $\delta^{18}O\text{-}NO_3^-$ signatures (Fig. S3), calculated using a mass-balance approach assuming no kinetic isotope fractionation (Walters and Michalski, 2016). $RO_2$ was assigned a $\delta^{18}O$ of 23.5‰, reflecting that O in $RO_2$ originates from molecular $O_2$ (Kroopnick and Craig, 1972). $O_3$ exhibits elevated $\delta^{18}O$ values ranging from 90 to 122‰ (Hastings et al., 2003). OH radicals were split into OH1 (−15 to 0‰) (Dubey et al., 1997), and OH2 (38 to 61‰). Daytime mechanisms included $P_{RO_2\text{-}OH1}$ (33−49‰), $P_{RO_2\text{-}OH2}$ (50−69‰), $P_{O_3\text{-}OH1}$ (55−81‰), and $P_{O_3\text{-}OH2}$ (73−102‰). Nighttime analysis focused on $P_{RO_2\text{-}het}$ (50−69‰) and $P_{O_3\text{-}het}$ (73−102‰), while retaining $P_{RO_2\text{-}OH1}$ to account for residual daytime nitrate that persists into the night. Sensitivity analyses regarding pathway exclusion are detailed in Supplementary Description S4, Tables S3 and S4."

**R1C9:** L 220- L227: Please provide the uncertainty for individual measurements and individual data points shown in Fig.2.

Response: Hourly concentrations of environmental parameters (Figure 2a−e) were obtained from the Taiwan Ministry of Environment, where the analytical uncertainties are governed by national

QA/QC standards. For isotope analysis (Figure 2f–h), the uncertainties for $\delta^{15}N$ and $\delta^{18}O$ of nitrate samples are generally less than 0.1‰, which is smaller than the symbol size. We have updated the caption of Figure 2 (Lines 204–205) as follows to clarify this:

> (Lines 204–205) "[…] Uncertainties for $\delta^{15}N$ and $\delta^{18}O$ measurements are generally less than 0.1‰ and are smaller than the symbol size."

**R1C10:** L260-263: The content is somewhat confusing and could benefit from clarification.

Response: This part was updated in section 3.3.1 in the revised manuscript (Lines 251–256) as follows:

> (Lines 251–256) "[…] This decline of $\delta^{15}N$ during the fog likely results from three concurrent processes under stagnant conditions. First, stagnant conditions suppressed the transport of $\delta^{15}N$-enriched urban plumes from nearby source regions. Second, continuous exchange between gas-phase $NH_3$ and $pNH_4^+$ shifts the particle phase toward the signature of the local $NH_3$ pool, which is depleted in $\delta^{15}N$ due to agricultural volatilization. Furthermore, wet deposition during fog may remove $^{15}N$-enriched particles, forcing the remaining $pNH_4^+$ to re-equilibrate with an increasingly $\delta^{15}N$-depleted gas phase. […]"

**R1C11:** L340-344: Despite the use of size-resolved isotope measurements, no clear or systematic dependence of $\delta^{15}N$ in $pNH_4^+$ or $pNO_3^-$ on particle size is observed (Fig. 6a, b), which limits the interpretive value of the size-segregated data.

Response: We thank the reviewer for this comment. We acknowledge that Figs. 6a and 6b do not reveal a systematic size-dependent trend in $\delta^{15}N$ or $\delta^{18}O$ of $pNO_3^-$. However, we suggest that the absence of such a trend is itself a meaningful finding, indicating that isotopic fractionation during gas-to-particle partitioning across size bins is not the dominant control on $\delta^{15}N$ variability at this site during the sampling period.

The interpretive strength of the size-segregated isotope approach becomes apparent when δ15N is examined in conjunction with $\delta^{18}O$ for $pNO_3^-$ (Fig. 6c). In this dual-isotope space, two distinct groupings emerge that would not be resolvable from bulk (non-size-resolved) measurements alone. One group, characterized by elevated $\delta^{18}O$ values, is consistent with $NO_3^-$ formation via $O_3$-initiated oxidation pathways, whereas another group exhibiting lower $\delta^{18}O$ values is more consistent with $RO_2$-initiated oxidation, indicative of photochemically processed or locally produced aerosol particles. The size-resolved sampling framework allows these isotopic signatures to be attributed to different particle size fractions, providing insight into the size-dependent source contributions and chemical processing histories that would otherwise be obscured in bulk measurements.

We have addressed this point in section 3.4.2 (Lines 374–387) of the revised manuscript as follows:

> (Lines 374–387) "Notably, no significant systematic size-dependent trend of $\delta^{18}O$-$NO_3^-$ on particle size was observed (Figs. 6a and 6b). The spatial heterogeneity of oxidants ($O_3$ and $RO_2$), coupled with the complex $HNO_3$ partitioning dynamics within the air parcel, likely erases any size-dependent isotopic pattern and daily variation (Figs. S12 and S13).

However, the $\delta^{15}N\text{-}NO_3^-$ vs. $\delta^{18}O\text{-}NO_3^-$ relationship (Fig. 6c) resolves two geochemically distinct regimes reflecting contrasting formation environments and aerosol histories. The higher $\delta^{18}O\text{-}NO_3^-$ (55−83‰) with enriched $\delta^{15}N\text{-}NO_3^-$ (−6 to 1‰) can be assigned as an urban/transported regime. Freshly emitted in metropolitan areas contributed to elevated $\delta^{15}N$, while $O_3$-driven oxidation leads to high $\delta^{18}O$ (Gobel et al., 2013). The observed lower $\delta^{18}O\text{-}NO_3^-$ (9−38‰) and depleted $\delta^{15}N\text{-}NO_3^-$ (−10 to −2‰) is assigned as a rural/fog regime. These signatures reflect $RO_2$-initiated oxidation and $\delta^{15}N$-depleted $NO_x$ from locally derived biogenic precursors or after extensive fractionation during transport, particularly under stagnant conditions. A moderate positive correlation ($r$ = 0.66) between $\delta^{18}O\text{-}NO_3^-$ and $\delta^{15}N\text{-}NO_3^-$ further highlights the intrinsic interplay between oxidation processes and nitrogen cycling at the site. These data demonstrate a $\delta^{18}O\text{-}NO_3^-$ and $\delta^{15}N\text{-}NO_3^-$ relationship that covers a broad isotopic range, spanning from the signatures observed at the Himalayan-Tibetan Plateau to those at regional background sites like Mt. Lulin (Fig. S14). ”

**References**


Chang, Y., Zhang, Y., Wang, Q., Shao, S., Bao, M., Zhang, C., and Lehmann, M. F.: Nitrogen isotope fractionation associated with ammonia gas-to-aerosol conversion and implications for determining isotopic source signatures and tracing atmospheric ammonium origins, Environ. Sci. Technol., 59, 22110-22121, https://doi.org/10.1021/acs.est.5c11271, 2025.

Chang, Y., Zhang, Y., Tian, C., Zhang, S., Ma, X., Cao, F., Liu, X., Zhang, W., Kuhn, T., and Lehmann, M. F.: Nitrogen isotope fractionation during gas-to-particle conversion of $NO_x$ to $NO_3^-$ in the atmosphere – implications for isotope-based $NO_x$ source apportionment, Atmos. Chem. Phys., 18, 11647-11661, https://doi.org/10.5194/acp-18-11647-2018, 2018.

Chen, T. Y., Chen, C. L., Chen, Y. C., Chou, C. C. K., Ren, H., and Hung, H. M.: Source apportionment and evolution of N-containing aerosols at a rural cloud forest in Taiwan by isotope analysis, Atmos. Chem. Phys., 22, 13001-13012, https://doi.org/10.5194/acp-22-13001-2022, 2022.

Dubey, M. K., Mohrschladt, R., Donahue, N. M., and Anderson, J. G.: Isotope specific kinetics of hydroxyl radical (OH) with water ($H_2O$): Testing models of reactivity and atmospheric fractionation, J. Phys. Chem. A, 101, 1494-1500, https://doi.org/10.1021/jp962332p, 1997.

Gobel, A. R., Altieri, K. E., Peters, A. J., Hastings, M. G., and Sigman, D. M.: Insights into anthropogenic nitrogen deposition to the North Atlantic investigated using the isotopic composition of aerosol and rainwater nitrate, Geophys. Res. Lett., 40, 5977-5982, https://doi.org/10.1002/2013GL058167, 2013.

Guha, T., Lin, C. T., Bhattacharya, S. K., Mahajan, A. S., Ou-Yang, C.-F., Lan, Y.-P., Hsu, S. C., and Liang, M.-C.: Isotopic ratios of nitrate in aerosol samples from Mt. Lulin, a high-altitude station in Central Taiwan, Atmos. Environ., 154, 53-69, https://doi.org/10.1016/j.atmosenv.2017.01.036, 2017.

Hall, S. J., Ogata, E. M., Weintraub, S. R., Baker, M. A., Ehleringer, J. R., Czimczik, C. I., and Bowling, D. R.: Convergence in nitrogen deposition and cryptic isotopic variation across urban and agricultural valleys in northern Utah, J. Geophys. Res.: Biogeosci., 121, 2340-2355, https://doi.org/10.1002/2016JG003354, 2016.

Hastings, M. G., Sigman, D. M., and Lipschultz, F.: Isotopic evidence for source changes of nitrate in rain at Bermuda, J. Geophys. Res.: Atmos., 108, 4790, https://doi.org/10.1029/2003JD003789, 2003.

Kawashima, H., Yoshida, O., and Suto, N.: Long-term source apportionment of ammonium in $PM_{2.5}$ at a suburban and a rural site using stable nitrogen isotopes, Environ. Sci. Technol., 57, 1268-1277, https://doi.org/10.1021/acs.est.2c06311, 2023.

Kroopnick, P. and Craig, H.: Atmospheric oxygen: Isotopic composition and solubility fractionation, Science, 175, 54-55, https://doi.org/10.1126/science.175.4017.54, 1972.

Kundu, S., Kawamura, K., and Lee, M.: Seasonal variation of the concentrations of nitrogenous species and their nitrogen isotopic ratios in aerosols at Gosan, Jeju Island: Implications for atmospheric processing and source changes of aerosols, J. Geophys. Res.: Atmos., 115, D20305, https://doi.org/10.1029/2009JD013323, 2010.

Lin, Y.-C., Zhang, Y.-L., Yu, M., Fan, M.-Y., Xie, F., Zhang, W.-Q., Wu, G., Cong, Z., and Michalski, G.: Formation mechanisms and source apportionments of airborne nitrate aerosols at a Himalayan-Tibetan Plateau site: Insights from nitrogen and oxygen isotopic compositions, Environ. Sci. Technol., 55, 12261-12271, https://doi.org/10.1021/acs.est.1c03957, 2021.

Moore, H.: The isotopic composition of ammonia, nitrogen dioxide and nitrate in the atmosphere, Atmos. Environ., 11, 1239-1243, https://doi.org/10.1016/0004-6981(77)90102-0, 1977.

Proemse, B. C., Mayer, B., Chow, J. C., and Watson, J. G.: Isotopic characterization of nitrate, ammonium and sulfate in stack $PM_{2.5}$ emissions in the Athabasca Oil Sands Region, Alberta, Canada, Atmos. Environ., 60, 555-563, https://doi.org/10.1016/j.atmosenv.2012.06.046, 2012.

Savard, M. M., Cole, A., Smirnoff, A., and Vet, R.: $\delta^{15}N$ values of atmospheric N species simultaneously collected using sector-based samplers distant from sources – Isotopic inheritance and fractionation, Atmos. Environ., 162, 11-22, https://doi.org/10.1016/j.atmosenv.2017.05.010, 2017.

Ti, C., Gao, B., Luo, Y., Wang, X., Wang, S., and Yan, X.: Isotopic characterization of $NH_x$-N in deposition and major emission sources, Biogeochemistry, 138, 85-102, https://doi.org/10.1007/s10533-018-0432-3, 2018.

Vicars, W. C., Morin, S., Savarino, J., Wagner, N. L., Erbland, J., Vince, E., Martins, J. M. F., Lerner, B. M., Quinn, P. K., Coffman, D. J., Williams, E. J., and Brown, S. S.: Spatial and diurnal variability in reactive nitrogen oxide chemistry as reflected in the isotopic composition of atmospheric nitrate: Results from the CalNex 2010 field study, J. Geophys. Res.: Atmos., 118, 10,567-510,588, https://doi.org/10.1002/jgrd.50680, 2013.

Walters, W. W. and Michalski, G.: Theoretical calculation of oxygen equilibrium isotope fractionation factors involving various $NO_y$ molecules, OH, and $H_2O$ and its implications for isotope variations in atmospheric nitrate, Geochim. Cosmochim. Acta, 191, 89-101, https://doi.org/10.1016/j.gca.2016.06.039, 2016.

Walters, W. W., Karod, M., Willcocks, E., Baek, B. H., Blum, D. E., and Hastings, M. G.: Quantifying the importance of vehicle ammonia emissions in an urban area of northeastern USA utilizing nitrogen isotopes, Atmos. Chem. Phys., 22, 13431-13448, https://doi.org/10.5194/acp-22-13431-2022, 2022.

We appreciate the reviewer for the useful comments. In the following, original reviewer comments are shown in black, our point-by-point responses are shown in blue, and updates on the manuscript are shown in blue and highlighted in yellow.

**Reviewer Comments to Author:**

**Reviewer: 2**

In their manuscript **"Size-resolved isotope analysis reveals anthropogenic reactive nitrogen transport and transformation in Taiwan mountain forests"**, authors conducted size-resolved isotope analysis of aerosol sampled at a mountain forest in Xitou, Taiwan to reveal sources and processes. The study is on a topic of relevance and general interest to the readers of ACP. Methodologically, studying reactive nitrogen species with isotopic techniques and source attribution modeling is not new. I am mostly concerned with the short period of sampling (8 days, 2 filter samples per day) and the lack of gas-phase nitrogen-containing species measurement, which makes it hard to form conclusive sources and formation pathways identification. Yet the data in the region of study during a prolonged fog is valuable, and the analyses were carried out comprehensively and rigorously. I am recommending a minor revision with detailed comments listed below.

**Specific comments:**

**R2C1:** In Introduction, Line 66-81, the scientific significance of the study is not well explained. It is stated that "relatively little is known about the sources and atmospheric processing of Nr in East Asian mountain forests", yet the authors later referred to Chen, T. Y. et al. (2022) that used the similar methodology (isotope signatures) at the same location. I'd love to see the authors further highlight the uniqueness of the location; for example, is Xitou a representative mountain forest area for East Asian, or at least for Taiwan (meteorologically wise, BVOC profile wise, urban-forest mixing wise)? Is Xitou known for abundant nitrogen-containing particles, mass concentration wise or fractional wise? Moreover, more information should be added to highlight the importance of aerosol chemistry under fog conditions (and summarize the current knowns and unknowns on aqueous phase processing etc.), followed by how your size-dependent isotopic approach could improve such understanding (see comment#5). This will enhance the scientific uniqueness of your study and can actually distinguish it from the previous one.

Response: We appreciate the reviewer for raising this point. Xitou is representing a mountain forest environment in Taiwan and East Asia, which is affected by local emissions and regional pollution transport by mountain-valley circulation and complex diurnal and seasonal variations in mixing layer heights. This part, as well as the Nr concentrations and the importance of aerosol chemistry under fog conditions, were updated in the revised manuscript in the introduction section (Lines 73−85) as follows:

> (Lines 73−85) "Xitou, a representative cloud forest in central Taiwan, serves as an ideal natural laboratory to address these gaps. Situated in a valley oriented toward urban regions, the site experiences predictable valley-mountain breeze circulations that transport anthropogenic plumes into a biogenic-rich environment where Nr accounts for

13−23% of $PM_{10}$ mass (Chen et al., 2021). This mixing vessel is characterized by frequent fog and persistent humidity, with a mean relative humidity (RH) above 80%. Fog droplets serve as a reactive aqueous medium, facilitating the dissolution of Nr species and accelerating secondary aerosol formation through aqueous-phase oxidation, thereby modifying aerosol hygroscopicity and chemical aging (Ervens, 2015). Specifically, aqueous-phase nitrate formation during fog proceeds via oxidation of $NO_2$ by ·OH radicals and heterogeneous hydrolysis of $N_2O_5$ on fog droplet surfaces. Furthermore, $NO_2$ disproportionation represents an additional pathway, a process enhanced by the larger radii of fog droplets compared to aerosol particles (Zhang et al., 2022; Lin et al., 2026; Yu et al., 2023). In addition, recent field research has demonstrated efficient nitrate formation during fog occurs mainly on fog interstitial aerosols through $NO_2$ and $N_2O_5$ hydrolysis, highlighting the importance of size-resolved characterization of aerosols under fog conditions (Xu et al., 2024). ”

**R2C2:** In Methods, Line 90, please justify your choice of the sampling period. Is April meteorologically favorable for foggy conditions or prone to higher ambient aerosol loadings or what? Is the week-long measurement representative enough for reaching your conclusions (e.g. those around Line 422)?

Response: We thank the reviewer for raising this point. We have added a justification for the choice of sampling period in the Methods section. The rationale addresses two aspects: the meteorological favorability for fog occurrence at Xitou in April, and the representativeness of the spring season in terms of aerosol loading and long-range transport influence.

- Fog conditions at Xitou in spring: Xitou is a mid-elevation cloud forest site in central Taiwan, situated in a mountainous subtropical island where forests cover more than 50% of the land area, and many highland sites experience over 100 fog days per year. Fog occurrence at Xitou is documented: Liang et al. (2009) reported 320 foggy days (visibility < 1000 m) at the site between April 2005 and March 2006, with the highest fog frequency concentrated between March and July (153 foggy days). Notably, the mean daily fog duration peaked in April at approximately 18.4 hours per day, making it the month with the most sustained fog cover within the year. Another study by Wey et al. (2011) also reported fog occurrence in April (14 foggy days; ~9 hours per day on average), though with lower frequency, likely reflecting interannual variability. Our own cloud ceilometer data collected at Xitou from 2017 to 2020 further corroborates that fog events occur frequently during spring (February–May, see Fig. R1 below). We therefore selected an April sampling window to maximize the likelihood of capturing fog processing of aerosols. It is also worth noting that while summer and winter have received more research attention at Xitou, spring, as a transitional season, is comparatively understudied, making our April dataset a useful contribution to the seasonal characterization of this site.
- Aerosol loading and long-range transport in spring: Beyond fog meteorology, April falls within a period of elevated aerosol loading in Taiwan. Ambient $PM_{10}$ and $PM_{2.5}$ concentrations in Taiwan typically reach their seasonal maxima in winter and remain comparably elevated through spring, before declining to their minima in summer. This elevated loading is in part driven by long-range transport: Taiwan is situated at the junction

of the East and South China Seas in the northwestern Pacific, flanked by the Chinese mainland to the northwest, Japan to the northeast, and the Philippines to the south. During winter and spring, anticyclonic systems originating from the Mongolian Plateau traverse the industrial corridors and megacity regions of eastern China, potentially entraining mineral dust and anthropogenic pollutants that are subsequently transported to Taiwan. In addition, biomass burning emissions from Southeast Asia can influence aerosol composition in the region during spring. Sampling in April thus captures a period of active long-range pollutant influence, providing an opportunity to examine how transported nitrogen species interact with local fog processing and gas–particle partitioning at the mountain site.

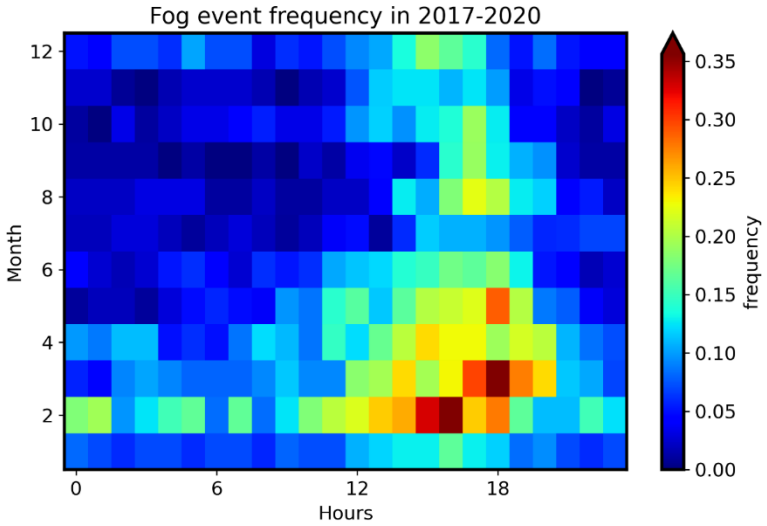


Figure R1. Monthly and diurnal distribution of fog event frequency at Xitou derived from ceilometer measurements during 2017–2020 (unpublished data, courtesy of co-authors).

On the representativeness of a week-long campaign, we acknowledge that a single week of observations carries inherent limitations for broader generalization. However, intensive short-term campaigns are a well-established approach in aerosol isotope studies, where the analytical demands of size-segregated impactor sampling and isotope ratio measurements preclude continuous year-round collection. The conclusions drawn around Line 422 are framed in terms of the processes observed during the campaign (e.g., fog aqueous-phase processing, transport signatures) rather than as climatological statements. We have clarified this point in the revised manuscript in the method section (Lines 97−99), section 3.4.2 (Lines 428−430), and the conclusions section (Lines 479−481) as follows:

> (Lines 97−99) “April represents the spring transition in Taiwan, a period characterized by frequent fog at Xitou, and a shift in aerosol loading from wintertime maxima to summertime minima.”
>
> (Lines 428−430) “[…] However, given the limited number of sampling days in this campaign, the relationship between nitrate formation pathways and pollution intensity warrants further investigation across seasons and contrasting meteorological conditions.”

(Lines 479–481) "[…] As these conclusions reflect processes observed during a one-week spring campaign, expanded measurements across multiple seasons and meteorological regimes would be needed to establish climatological representativeness. […]"

**R2C3:** In Methods, section 2.3.2, the inclusion and exclusion of certain pathways during daytime and nighttime analysis reads arbitrary. It is recommended to provide results of sensitivity tests for the mentioned inclusion and exclusion to see if such decisions alter the results or not in the SI.

Response: We thank the reviewer for the suggestion. To justify the selection of pathways for the nighttime nitrate formation analysis, we performed a sensitivity analysis comparing three different model configurations (C0–C2):

- C0 (original): $P_{RO_2\text{-}OH1}$, $P_{RO_2\text{-}het}$, and $P_{O_3\text{-}het}$
- C1 (full): $P_{RO_2\text{-}OH1}$, $P_{RO_2\text{-}OH2}$, $P_{RO_2\text{-}het}$, $P_{O_3\text{-}OH1}$, $P_{O_3\text{-}OH2}$, $P_{O_3\text{-}het}$
- C2 (nighttime only): $P_{RO_2\text{-}het}$ and $P_{O_3\text{-}het}$,

The results demonstrate that C0 provides the best fit. In addition, excluding P1a (C2) leads to a sharp increase in the absolute differentiation (averaged error) from 4.34‰ to 14‰, as these models fail to capture observed low $\delta^{18}O$ values (< 40‰). Furthermore, the full model (C1) did not improve accuracy (averaged error of 5.65‰) and introduced unnecessary complexity due to the identical $^{18}O$ signatures of $P_{RO_2\text{-}OH2}/P_{RO_2\text{-}het}$ and $P_{O_3\text{-}OH2}/P_{O_3\text{-}het}$. Consequently, C0 was selected as the optimized setting.

| Sample ID | Measured $\delta^{18}O$ (‰) | Reconstructed $\delta^{18}O$ (‰) (absolute difference, ‰) | | |
|---|---|---|---|---|
| | | C0 (4.34) | C1 (5.65) | C2 (14) |
| 17N | 35.86 | 43.18 (7.32) | 44.99 (9.13) | 60.05 (24.19) |
| 18N | 33.81 | 42.71 (8.90) | 44.54 (10.72) | 59.99 (26.18) |
| 19N | 73.27 | 72.48 (0.79) | 71.91 (1.36) | 74.13 (0.86) |
| 20N | 31.94 | 42.42 (10.47) | 44.03 (12.09) | 59.97 (28.02) |
| 21N | 69.49 | 69.29 (0.20) | 69.02 (0.47) | 70.14 (0.65) |
| 22N | 43.37 | 46.01 (2.65) | 48.26 (4.89) | 60.30 (16.93) |
| 23N | 64.79 | 64.85 (0.06) | 65.65 (0.86) | 65.56 (1.17) |

Contribution of each pathway in C0 (and C1):

| Sample ID | Measured $\delta^{18}O$ (‰) | Fractional contribution | | | | | |
|---|---|---|---|---|---|---|---|
| | | $P_{RO_2\text{-}OH1}$ | $P_{RO_2\text{-}OH2}$ | $P_{RO_2\text{-}het}$ | $P_{O_3\text{-}OH1}$ | $P_{O_3\text{-}OH2}$ | $P_{O_3\text{-}het}$ |
| 17N | 35.86 | 0.91(0.85) | (0.03) | 0.06(0.04) | (0.04) | (0.02) | 0.03(0.02) |
| 18N | 33.81 | 0.93(0.87) | (0.03) | 0.05(0.03) | (0.03) | (0.02) | 0.03(0.02) |
| 19N | 73.27 | 0.16(0.09) | (0.17) | 0.27(0.14) | (0.14) | (0.23) | 0.58(0.23) |
| 20N | 31.94 | 0.94(0.88) | (0.03) | 0.04(0.03) | (0.03) | (0.02) | 0.02(0.02) |
| 21N | 69.49 | 0.19(0.12) | (0.18) | 0.33(0.16) | (0.16) | (0.19) | 0.48(0.19) |
| 22N | 43.37 | 0.80(0.73) | (0.06) | 0.14(0.07) | (0.07) | (0.03) | 0.06(0.03) |
| 23N | 64.79 | 0.24(0.16) | (0.18) | 0.41(0.19) | (0.20) | (0.13) | 0.36(0.14) |

This point was updated in section 2.3.2 of the revised manuscript (Lines 182−183) and in Description 3, Tables S3 and S4 of SI as follows:

(Lines 182−183) "[…] Sensitivity analyses regarding pathway exclusion are detailed in Supplementary Description S4, Tables S3 and S4."

**"Description S4. Sensitivity analyses on the nitrate formation pathway**

Sensitivity analyses were performed to compare three different model configurations (C0–C2):

- C0 (main text): $P_{RO_2\text{-}OH1}$, $P_{RO_2\text{-}het}$, and $P_{O_3\text{-}het}$
- C1 (full): $P_{RO_2\text{-}OH1}$, $P_{RO_2\text{-}OH2}$, $P_{RO_2\text{-}het}$, $P_{O_3\text{-}OH1}$, $P_{O_3\text{-}OH2}$, $P_{O_3\text{-}het}$
- C2 (nighttime only): $P_{RO_2\text{-}het}$ and $P_{O_3\text{-}het}$,

The results demonstrate that C0 provides the best fit. In addition, excluding P1a (C2) leads to a sharp increase in the absolute differentiation (averaged error) from 4.34‰ to 14‰, as these models fail to capture observed low $\delta^{18}O$ values (< 40‰) (Table S3). Furthermore, the full model (C1) did not improve accuracy (averaged error of 5.65‰) and introduced unnecessary complexity due to the identical $^{18}O$ signatures of $P_{RO_2\text{-}OH2}/P_{RO_2\text{-}het}$ and $P_{O_3\text{-}OH2}/P_{O_3\text{-}het}$ (Figure S4). Consequently, C0 was selected as the optimized setting."

**Table S3.** Reconstructed $\delta^{18}O$ (‰) from MixSIAR results of C0, C1, and C2 scenarios.

| Sample ID | Measured $\delta^{18}O$ (‰) | Reconstructed $\delta^{18}O$ (‰) (absolute difference, ‰) | | |
|---|---|---|---|---|
| | | C0 (4.34) | C1 (5.65) | C2 (14) |
| 17N | 35.86 | 43.18 (7.32) | 44.99 (9.13) | 60.05 (24.19) |
| 18N | 33.81 | 42.71 (8.90) | 44.54 (10.72) | 59.99 (26.18) |
| 19N | 73.27 | 72.48 (0.79) | 71.91 (1.36) | 74.13 (0.86) |
| 20N | 31.94 | 42.42 (10.47) | 44.03 (12.09) | 59.97 (28.02) |
| 21N | 69.49 | 69.29 (0.20) | 69.02 (0.47) | 70.14 (0.65) |
| 22N | 43.37 | 46.01 (2.65) | 48.26 (4.89) | 60.30 (16.93) |
| 23N | 64.79 | 64.85 (0.06) | 65.65 (0.86) | 65.56 (1.17) |

**Table S4.** Fractional contribution of each nitrate formation pathway in C0 (and C1).

| Sample ID | Measured $\delta^{18}O$ (‰) | Fractional contribution of C0 (and C1) | | | | | |
|---|---|---|---|---|---|---|---|
| | | $P_{RO_2\text{-}OH1}$ | $P_{RO_2\text{-}OH2}$ | $P_{RO_2\text{-}het}$ | $P_{O_3\text{-}OH1}$ | $P_{O_3\text{-}OH2}$ | $P_{O_3\text{-}het}$ |
| 17N | 35.86 | 0.91(0.85) | (0.03) | 0.06(0.04) | (0.04) | (0.02) | 0.03(0.02) |
| 18N | 33.81 | 0.93(0.87) | (0.03) | 0.05(0.03) | (0.03) | (0.02) | 0.03(0.02) |
| 19N | 73.27 | 0.16(0.09) | (0.17) | 0.27(0.14) | (0.14) | (0.23) | 0.58(0.23) |
| 20N | 31.94 | 0.94(0.88) | (0.03) | 0.04(0.03) | (0.03) | (0.02) | 0.02(0.02) |
| 21N | 69.49 | 0.19(0.12) | (0.18) | 0.33(0.16) | (0.16) | (0.19) | 0.48(0.19) |
| 22N | 43.37 | 0.80(0.73) | (0.06) | 0.14(0.07) | (0.07) | (0.03) | 0.06(0.03) |
| 23N | 64.79 | 0.24(0.16) | (0.18) | 0.41(0.19) | (0.20) | (0.13) | 0.36(0.14) |

**R2C4:** In Results, Line 270-284 and Figure 4 are too speculative to me. I am not convinced how useful it is to have three independent linear regression lines on such limited data points. Moreover, grouping the clear data into <~1 micron and >1 micron reads arbitrary and is too mechanical. The hypotheses and suggested explanations were not supported by any ancillary or referable data, and I am not sure if the trend or differences are statistically significant. For

example, if the cutoff is not at 1 micron but at 1.5 or 2 micron, will the revealed increase go from 7.14 to 16.08 per mil? Will the $\delta^{15}N\text{-}NH_4^+$ values of this group really be lower then? When you say "coarse particles (1−10 μm) are likely produced from urban areas…that were subsequently transported to the sampling site", does your wind data support such a hypothesis? I agree that a bell-shaped pattern is revealed in Figure 4 and it becomes less apparent during the fog, but the corresponding discussions shall be revised with more supporting evidence.

Response: We thank the reviewer for the critical comment. We updated Figure 4 and the descriptions for Figure 4 in section 3.3.1 (Lines 264−293) of the revised manuscript as follows:

> (Lines 264−293) "Under clear conditions (excluding 19N and 21D), the size-resolved $\delta^{15}N\text{-}NH_4^+$ distribution revealed a bell-shaped distribution (Fig. 4). Values peaked at ~15‰ in the accumulation mode (~0.5−2 μm) and decreased to ~7‰ in both the ultrafine and coarse particles. This pattern reflects a transition between local emissions and aged, transported aerosols. For ultrafine mode (<0.5 μm), particles maintain isotopic equilibrium with the local $NH_3$ pool, dominated by $\delta^{15}N$-depleted residual $NH_3$ or volatilization sources (typically −28.3‰ to −17.6‰). For accumulation-mode (~0.5–2 μm), particles preserve the signatures of lower-elevation anthropogenic emission regions. Here, combustion-derived $NH_3$ (typically −8.2‰ to 1.8‰) reacts with $H_2SO_4$ to form non-volatile ammonium sulfate and ammonium bisulfate. Unlike ammonium nitrate, which is more volatile and easily re-equilibrates with gas-phase $NH_3$ during transport, sulfate-bound $NH_4^+$ is more resistant to isotopic re-equilibration, allowing it to act as a conservative tracer of urban source signatures during upslope transport (Wu et al., 2022). For the coarse mode (> 2 μm), particles are likely dominated by mineral dust and sea salt and present a substantially weaker thermodynamic sink for $NH_3$ absorption compared to acidic fine-mode sulfate aerosols (Fig. S6) (Pye et al., 2020). Therefore, $NH_4^+$ in this mode likely maintains a dynamic equilibrium with local gas-phase $NH_3$, which becomes progressively depleted in $^{15}N$ as the air mass ages.
>
> During fog, the bell-shaped distribution flattened significantly. Weakened wind suppressed the upslope transport of enriched anthropogenic pollutants, while enhanced aqueous-phase interaction promoted uniform isotopic re-equilibrium across all sizes. The high $NO_3^-$ concentration from aqueous chemistry can also promote the local isotopically depleted $NH_3$ partitioning into the particle phase, dampening the size-dependent isotopic gradient.
>
> The flat $\delta^{15}N\text{-}NH_4^+$ size distribution was also observed on 19N and 21D. For 19N, it is likely a legacy effect of the preceding fog period (18D, 18N, and 19D). The $NH_3$ pool remained isotopically depleted from sustained fog-driven scavenging and re-equilibration, and regional transport had not yet replenished the accumulation-mode signal. However, high sub-micrometer $NO_3^-$ concentration (Fig. S4) suggests that fog-like aqueous chemistry persisted, maintaining isotopic signatures similar to 18D. Conversely, the flat distribution on 21D reflects a distinct source influence. HYSPLIT back-trajectories (Fig. S7) indicate that the air parcel traveled through agricultural regions characterized by heavily depleted $NH_3$ (e.g., livestock waste, −28.3‰ to −17.6‰). The partitioning of this isotopically light $NH_3$ during transit effectively erased the characteristic accumulation-mode enrichment.

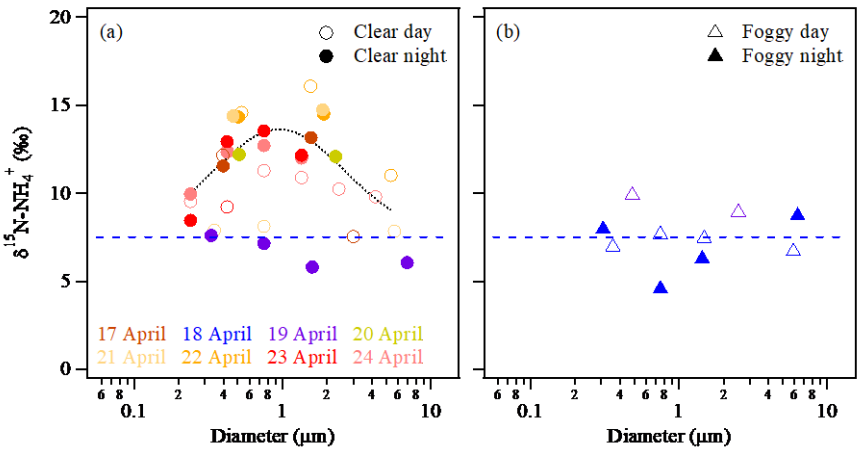


Figure 4. $\delta^{15}N$ of size-segregated $pNH_4^+$ during (a) clear and (b) foggy conditions. The dashed blue line indicates the mean $\delta^{15}N\text{-}NH_4^+$ for foggy periods. The dotted curve represents LogNormal distribution fits for clear conditions, excluding 19N and 21D, where no distinct bell-shaped size dependence was identified."

**R2C5:** Figures corresponding to results discussed in sections 3.4.2 and 3.4.3 are all in the SI. I'd suggest combining the two sections into one and bringing Figure S14 into the main manuscript for better interpretation. You may consider discussing the shifts in formation pathways (PXa, PXb) in a more descriptive, mechanistic language (Line 380 onward). I'd also suggest highlighting the importance of your pathway identifications (even though with uncertainties and assumptions) for improving the understanding of the particulate nitrate formation. Recent studies coupling the organonitrates formation during day and night with varied meteorological conditions, such as a few listed below, could be used for your reference and to put your findings into the broader picture:

Guo et al., 2024 (https://doi.org/10.1016/j.atmosenv.2024.120362)

Ward et al., 2025 (https://doi.org/10.1126/sciadv.adt8957)

Murphy et al., 2025 (https://doi.org/10.1021/acsestair.5c00206).

Response: We thank the reviewer for this suggestion. Sections 3.4.2 and 3.4.3 have been combined into a single section in the revised manuscript, and Figure S14 has been promoted to Figure 7. We have also updated the discussion of shifts in formation pathways and added two new paragraphs: one elaborating on the significance of pathway identification, and another addressing organon nitrate formation. This point was updated in the revised manuscript in section 3.4.2 (Lines 394−446) as follows:

> (Lines 394−446) "Formation pathways of $pNO_3^-$ were quantitatively analyzed using the MixSIAR framework based on $\delta^{18}O\text{-}NO_3^-$ values, as shown in Fig. 7a. During daytime periods characterized by low $\delta^{18}O\text{-}NO_3^-$ values (31−41‰) and low CO concentrations (< 0.22ppm, 17D, 19D, and 23D), $P_{RO_2\text{-}OH1}$ accounted for 82−92% of $pNO_3^-$ formation (Fig. 7a and 7b). These conditions are consistent with periods with limited influence from urban air masses, suggesting the dominance of local $RO_2$ oxidation processes. In contrast, during daytime with higher $\delta^{18}O\text{-}NO_3^-$ values (63−70‰) and to elevated CO

concentrations (0.24−0.27 ppm, 18D, 21D, 22D), the dominant pathways shifted toward $P_{RO_2\text{-}OH2}$, $P_{O_3\text{-}OH1}$, and $P_{O_3\text{-}OH2}$, contributing an average of 29±1%, 27±3%, and 28±5%, respectively. This shift could probably reflect the enhanced transport of urban air masses enriched in $O_3$ and $NO_x$ precursors.

Although nighttime nitrate formation is theoretically dominated by heterogeneous reactions, our results reveal a more complex process. On nights with elevated $\delta^{18}O\text{-}NO_3^-$ values, heterogeneous pathways ($P_{RO_2\text{-}het}$ and $P_{O_3\text{-}het}$) were the dominant contributors, accounting for 33±6% and 47±9% of $pNO_3^-$ formation on 19N, 21N, 23N. In contrast, on nights with lower $\delta^{18}O\text{-}NO_3^-$ values (32−43‰, 17N, 18N, 20N, and 22N), $P_{RO_2\text{-}OH1}$ remained a major contributor, accounting for 80−94% of formation. This high $P_{RO_2\text{-}OH1}$ might stem from the residual $pNO_3^-$ from daytime, or nighttime ·OH generated via reactions between $O_3$ and alkenes/terpenes (Kroll et al., 2001; Aschmann et al., 2002). The weak night-to-night covariation between $\delta^{18}O\text{-}NO_3^-$ and CO concentrations further suggests that nighttime nitrate isotope signatures are governed by the interplay among fog processing, reduced advection, and heterogeneous chemistry, rather than transport intensity alone.

A distinct shift in nitrate formation pathways was observed during the fog. On 18D, high $\delta^{18}O\text{-}NO_3^-$ values (70‰) and elevated CO concentrations (0.24 ppm) were associated with the dominance of $P_{RO_2\text{-}OH2}$ (30±20%) and $P_{O_3\text{-}OH2}$ (36±16%), indicating that $O_3$ from transported urban precursors remained active (Fig. S15). As fog intensified during 18N and persisted into 19D, $\delta^{18}O\text{-}NO_3^-$ values decreased sharply to ~34‰, and $P_{RO_2\text{-}OH1}$ became dominant (93±5% on 18N, and 90±5% on 19D). This transition is driven by two coupled effects: (1) the attenuation of incoming solar radiation suppresses $O_3$ photolysis and thereby reduces the availability of high-$\delta^{18}O$ oxidants, and (2) the scavenging of long-range transport by wet deposition diminishes the influx of urban $NO_x$ and $O_3$. Together, these foggy conditions favor locally derived low-$\delta^{18}O$ $RO_2$ cycling as the predominant oxidant driving nitrate formation.

Distinguishing the relative contributions helps clarify how nitrate formation processes vary with air mass origin, photochemical activity, and fog processing, which is directly relevant to emission control strategies since the efficacy of nitrate reduction depends on the dominant oxidation pathway. At the global scale, model estimated that the $NO_2$ + ·OH (same as our $P_{O_3\text{-}OH1}/P_{O_3\text{-}OH2}$) and $N_2O_5$ hydrolysis (same as our $P_{RO_2\text{-}het}/P_{O_3\text{-}het}$) pathways each contributed approximately 41% to tropospheric nitrate formation (Alexander et al., 2020), while observation studies in both urban and mountain environments suggest that heterogeneous pathways become more important for nitrate formation under elevated pollution levels (Fan et al., 2020; Lin et al., 2021). The pathway apportionment presented here provides finer resolution than bulk gas-phase/heterogeneous partitioning by explicitly distinguishing $RO_2$- from $O_3$-initiated formation, which can be useful in regions where $RO_2$ oxidation dominates. However, given the limited number of sampling days in this campaign, the relationship between nitrate formation pathways and pollution intensity warrants further investigation across seasons and contrasting meteorological conditions.

Beyond inorganic $HNO_3$ formation, the total particulate nitrogen budget includes particulate organic nitrate ($pON$) species, which can account for 17−31% of total

particulate nitrogen (Yu et al., 2024) in mixed urban-biogenic environments, and up to 50% observed in urban plumes (Murphy et al., 2025). *p*ON forms via the reaction of NO with $RO_2$ (NO + $RO_2$ → $RONO_2$) during the day, and $NO_3$ with alkenes and biogenic VOC at night ($NO_3$ + R → $RONO_2$) (Murphy et al., 2025; Ward et al., 2025; Guo et al., 2024). These mechanisms operate through the same $RO_2$- and $NO_3$-driven pathways identified here ($P_{RO_2\text{-}OH1}$ / $P_{RO_2\text{-}OH2}$ and $P_{RO_2\text{-}het}$/$P_{O_3\text{-}het}$, respectively), suggesting that the oxidation chemistry inferred from $\delta^{18}O\text{-}NO_3^-$ signatures at Xitou also drives concurrent *p*ON production. Because isotope analysis in this study assumes TN comprises only $NO_3^-$ and $NH_4^+$, organic nitrogen contribution could bias the derived $\delta^{15}N\text{-}NH_4^+$ toward the signature of *p*ON. While this was partially mitigated by excluding samples with low $[NH_4^+]$ (<60% of ([TN]−[NN])), future research should prioritize direct $\delta^{15}N\text{-}NH_4^+$ measurement, which would enable the estimation of organic nitrate isotopes via residual mass balance (i.e., [ON] = [TN] – $[NH_4^+]$ – $[NO_3^-]$) and provide a more complete characterization of the Nr budget in mountain forest environments.

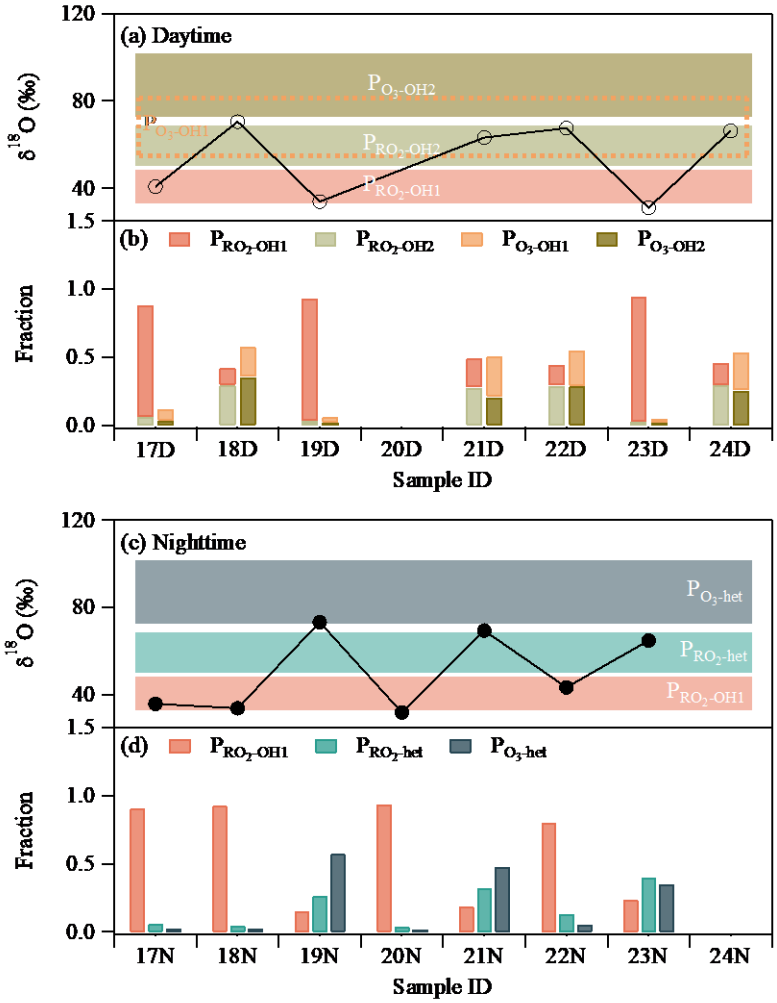


**Figure 7. Contributions of nitrate formation pathways estimated by MixSIAR. (a, c) Measured $\delta^{18}O\text{-}NO_3^-$ values with the corresponding $\delta^{18}O$ ranges of potential formation pathways. (b, d) estimated fractional contributions of these pathways.**”

**Technical corrections:**

**R2C6:** In Figure 6a, I am not sure if the regression line is needed given how scattered the data are.

Response: We have removed the regression line in Figure 6a in the revised manuscript to avoid over-interpreting the relationship between these variables.

**R2C7:** Same as above for Figure S15.

Response: The regression line in Figure S15 has also been removed in the revised manuscript.

**R2C8:** What's your take on larger particles being more neutral and smaller being more acidic from your Figure S6? Is it consistent with your hypothesis that more coarse particles were transported from the urban area?

Response: We thank the reviewer for this comment. Figure S6 is based on FTIR-derived ionic concentrations, which show a size-dependent acidity gradient with finer particles appearing more acidic and coarser particles more neutral. However, we note that IC-based measurements, which provide more quantitatively reliable ionic concentrations, do not show a clear systematic acidity gradient across size fractions (Fig. S6 in the revised manuscript). Given the known limitations of FTIR for quantitative ion concentration retrieval compared to IC, we consider the IC-based assessment more robust for evaluating particle neutralization state. In the IC-based data (Fig. S6), fine particles are approximately charge-balanced, while coarse particles exhibit an apparent anion excess, likely attributable to unmeasured crustal or sea-salt cations (e.g., $Na^+$, $Ca^{2+}$, $Mg^{2+}$) which were not quantified in this study. We've updated Figure S6 and the description about this part in section 3.3.1 (Lines 264–277) of the revised manuscript as follows:

(Figure S6)

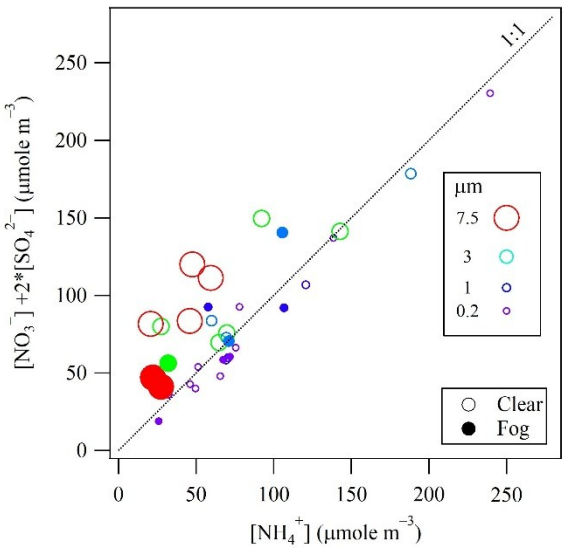


**Figure S6.** Scatter plot of $[NO_3^-] + 2*[SO_4^{2-}]$ versus $[NH_4^+]$ measured by ion chromatography during the observation period.

(Lines 264–277) "Under clear conditions (excluding 19N and 21D), the size-resolved $\delta^{15}N\text{-}NH_4^+$ distribution revealed a bell-shaped distribution (Fig. 4). Values peaked at ~15‰ in the accumulation mode (~0.5–2 μm) and decreased to ~7‰ in both the ultrafine and coarse particles. This pattern reflects a transition between local emissions and aged, transported aerosols. For ultrafine mode (<0.5 μm), particles maintain isotopic equilibrium with the local $NH_3$ pool, dominated by $\delta^{15}N$-depleted residual $NH_3$ or volatilization sources (typically −28.3‰ to −17.6‰). For accumulation-mode (~0.5–2 μm), particles preserve the signatures of lower-elevation anthropogenic emission regions. Here, combustion-derived $NH_3$ (typically −8.2‰ to 1.8‰) reacts with $H_2SO_4$ to form non-volatile ammonium sulfate and ammonium bisulfate. Unlike ammonium nitrate, which is more volatile and easily re-equilibrates with gas-phase $NH_3$ during transport, sulfate-bound $NH_4^+$ is more resistant to isotopic re-equilibration, allowing it to act as a conservative tracer of urban source signatures during upslope transport (Wu et al., 2022). For the coarse mode (> 2 μm), particles are likely dominated by mineral dust and sea salt and present a substantially weaker thermodynamic sink for $NH_3$ absorption compared to acidic fine-mode sulfate aerosols (Fig. S6) (Pye et al., 2020). Therefore, $NH_4^+$ in this mode likely maintains a dynamic equilibrium with local gas-phase $NH_3$, which becomes progressively depleted in $^{15}N$ as the air mass ages."

**References**


Alexander, B., Sherwen, T., Holmes, C. D., Fisher, J. A., Chen, Q., Evans, M. J., and Kasibhatla, P.: Global inorganic nitrate production mechanisms: comparison of a global model with nitrate isotope observations, Atmos. Chem. Phys., 20, 3859-3877, https://doi.org/10.5194/acp-20-3859-2020, 2020.

Aschmann, S. M., Arey, J., and Atkinson, R.: OH radical formation from the gas-phase reactions of $O_3$ with a series of terpenes, Atmos. Environ., 36, 4347-4355, https://doi.org/10.1016/S1352-2310(02)00355-2, 2002.

Chen, C.-L., Chen, T.-Y., Hung, H.-M., Tsai, P.-W., Chou, C. C. K., and Chen, W.-N.: The influence of upslope fog on hygroscopicity and chemical composition of aerosols at a forest site in Taiwan, Atmos. Environ., 246, 118150, https://doi.org/10.1016/j.atmosenv.2020.118150, 2021.

Ervens, B.: Modeling the processing of aerosol and trace gases in clouds and fogs, Chem. Rev., 115, 4157-4198, https://doi.org/10.1021/cr5005887, 2015.

Fan, M.-Y., Zhang, Y.-L., Lin, Y.-C., Cao, F., Zhao, Z.-Y., Sun, Y., Qiu, Y., Fu, P., and Wang, Y.: Changes of emission sources to nitrate aerosols in Beijing after the clean air actions: Evidence from dual isotope compositions, J. Geophys. Res.: Atmos., 125, e2019JD031998, https://doi.org/10.1029/2019JD031998, 2020.

Guo, F., Bui, A. A. T., Schulze, B. C., Dai, Q., Yoon, S., Shrestha, S., Wallace, H. W., Sanchez, N. P., Alvarez, S., Erickson, M. H., Sheesley, R. J., Usenko, S., Flynn, J., and Griffin, R. J.: Airmass history, night-time particulate organonitrates, and meteorology impact urban SOA formation rate, Atmos. Environ., 322, 120362, https://doi.org/10.1016/j.atmosenv.2024.120362, 2024.

Kroll, J. H., Clarke, J. S., Donahue, N. M., Anderson, J. G., and Demerjian, K. L.: Mechanism of $HO_x$ formation in the gas-phase ozone−alkene reaction. 1. Direct, pressure-dependent measurements of prompt OH yields, J. Phys. Chem. A, 105, 1554-1560, https://doi.org/10.1021/jp002121r, 2001.

Liang, Y.-L., Lin, T.-C., Hwong, J.-L., Lin, N.-H., and Wang, C.-P.: Fog and Precipitation Chemistry at a Mid-land Forest in Central Taiwan, J. Environ. Qual., 38, 627-636, https://doi.org/10.2134/jeq2007.0410, 2009.

Lin, Y.-C., Zhang, Y.-L., Yu, M., Fan, M.-Y., Xie, F., Zhang, W.-Q., Wu, G., Cong, Z., and Michalski, G.: Formation mechanisms and source apportionments of airborne nitrate aerosols at a Himalayan-Tibetan Plateau site: Insights from nitrogen and oxygen isotopic compositions, Environ. Sci. Technol., 55, 12261-12271, https://doi.org/10.1021/acs.est.1c03957, 2021.

Lin, Z., Ji, X., Xu, L., Chen, G., Yang, C., Zhang, K., Zhang, F., Li, L., Chen, Y., and Chen, J.: Enhanced $NO_2$-driven multiphase formation of particulate nitrate and sulfate under high-humidity conditions, npj Clim. Atmos. Sci., 9, 76, https://doi.org/10.1038/s41612-026-01352-5, 2026.

Murphy, S. E., Buenconsejo, R. S., Draper, D. C., Crounse, J. D., Baliaka, H. D., Ward, R. X., Schulze, B. C., Rezgui, S. P., Ball, K., Susskind, T., Kappaganthula, G., and Wennberg, P. O.: Multi-functional organic nitrogen in the Los Angeles Air Basin, ACS ES&T Air, 2, 2009-2027, https://doi.org/10.1021/acsestair.5c00206, 2025.

Pye, H. O. T., Nenes, A., Alexander, B., Ault, A. P., Barth, M. C., Clegg, S. L., Collett Jr, J. L., Fahey, K. M., Hennigan, C. J., Herrmann, H., Kanakidou, M., Kelly, J. T., Ku, I. T., McNeill, V. F., Riemer, N., Schaefer, T., Shi, G., Tilgner, A., Walker, J. T., Wang, T., Weber, R., Xing, J., Zaveri, R. A., and Zuend, A.: The acidity of atmospheric particles and clouds, Atmos. Chem. Phys., 20, 4809-4888, https://doi.org/10.5194/acp-20-4809-2020, 2020.

Ward, R. X., Baliaka, H. D., Schulze, B. C., Kerr, G. H., Crounse, J. D., Hasheminassab, S., Bahreini, R., Dillner, A. M., Russell, A., Ng, N. L., Wennberg, P. O., Flagan, R. C., and Seinfeld, J. H.: Poorly quantified trends in ammonium nitrate remain critical to understand future urban aerosol control strategies, Science Advances, 11, eadt8957, https://doi.org/10.1126/sciadv.adt8957, 2025.

Wey, T.-H., Lai, Y.-J., Chang, C.-S., Shen, C.-W., Hong, C.-Y., Wang, Y.-N., and Chen, M.-C.: Preliminary Studies on Fog Characteristics at Xitou Region of Central Taiwan, Jour. Exp. For. Nat. Taiwan Univ., 25, 149-160, https://doi.org/10.6542/EFNTU.201106_25(2).0006, 2011.

Wu, C., Cao, C., Li, J., Lv, S., Li, J., Liu, X., Zhang, S., Liu, S., Zhang, F., Meng, J., and Wang, G.: Different physicochemical behaviors of nitrate and ammonium during transport: a case study on Mt. Hua, China, Atmos. Chem. Phys., 22, 15621-15635, https://doi.org/10.5194/acp-22-15621-2022, 2022.

Xu, W., Kuang, Y., Xu, W., Liu, L., Xu, H., Wang, X., Liu, Y., Cheng, H., Zhang, X., Zhai, M., Liu, C., Liang, L., Zhang, G., Luo, B., Tao, J., Liu, J., Zhao, H., Ren, S., Zhou, G., Liu, P., Xu, X., and Sun, Y.: Efficient nitrate formation in fog events implicates fog interstitial aerosols as

significant drivers of atmospheric chemistry, Environ. Sci. Technol., 58, 22298-22311, https://doi.org/10.1021/acs.est.4c09078, 2024.

Yu, H.-R., Zhang, Y.-L., Cao, F., Zhao, Z.-Y., Fan, M.-Y., and Yang, X.-Y.: Fog event is possibly a source rather than a sink of atmospheric nitrate aerosols: Insights from isotopic measurements in Nanjing, China, Appl. Geochem., 155, 105721, https://doi.org/10.1016/j.apgeochem.2023.105721, 2023.

Yu, X., Li, Q., Liao, K., Li, Y., Wang, X., Zhou, Y., Liang, Y., and Yu, J. Z.: New measurements reveal a large contribution of nitrogenous molecules to ambient organic aerosol, npj Clim. Atmos. Sci., 7, 72, https://doi.org/10.1038/s41612-024-00620-6, 2024.

Zhang, G., Hu, X., Sun, W., Yang, Y., Guo, Z., Fu, Y., Wang, H., Zhou, S., Li, L., Tang, M., Shi, Z., Chen, D., Bi, X., and Wang, X.: A comprehensive study about the in-cloud processing of nitrate through coupled measurements of individual cloud residuals and cloud water, Atmos. Chem. Phys., 22, 9571-9582, https://doi.org/10.5194/acp-22-9571-2022, 2022.